Chapter 3

Measurement Procedures

The group of measurements necessary to characterize both the color and surface finish of an object is called the *measurement of appearance* of an object [102]. This group of measurements involves the spectral energy distribution of propagated light, measured in terms of reflectance and transmittance, and the spatial energy distribution of that light, measured in terms of BRDF and BTDF.

The variations in the spectral distribution of the propagated light affect appearance characteristics such as hue, lightness and saturation [102]. Hue is the attribute of color perception by means which an object is judged to be red, yellow, green, blue, purple and so forth. Lightness is the attribute by which white objects are distinguished from gray objects and light from dark colored objects. Finally, saturation is the attribute that expresses the degree of departure from the gray of the same lightness.

The changes in the spatial distribution of the propagated light affect appearance characteristics such as gloss, reflection haze, transmission haze, luster and translucency. The reflection haze corresponds to the scattering of reflected light in directions near that of specular reflection by a specimen having a glossy surface [102]. The transmission haze corresponds to the scattering of light within or at the surface of a nearly clear specimen, which is responsible for cloudy appearance seen by transmission [102]. Finally, the luster, or contrast gloss, as described by Hunter and Harold [102], corresponds to the gloss associated with contrasts of bright and less bright adjacent areas of the surface of an object. Luster increases with increased ratio between light reflected in the specular direction and that reflected in those diffuse directions which are adjacent to the specular direction.

Greenberg *et al.* [86] proposed a framework to test, validate and improve the fidelity and efficiency of computer graphics algorithms, which is composed of three stages, namely local light scattering models, light transport simulations and image display procedures. They emphasized the importance of performing comparisons between simulations and actual measurements so that simulations can be used in a predictive manner. According to their paradigm, it is of fundamental importance that at each stage simulations are compared with measured experiments. Actual measurements of reflectance and transmittance are performed using spectrophotometers, and actual measurements of BRDF and BTDF are performed using goniophotometers [102, 110]. These devices are important basic tools for fundamental research in colorimetry [135], solar engineering [61], remote sensing [52, 108] and plant biochemistry [27, 108]. In this chapter we discuss the computer simulations of such devices, henceforth called virtual measurement devices. The use of these virtual devices enables us to measure the spectral data generated from computer models and allows us to perform experiments at different sampling resolutions, which are essential requirements for rendering applications as pointed out by Lalonde and Fournier [126].

Two applications of virtual measurements are especially relevant for biologically and physically-based rendering. The first application corresponds to virtual measurements aimed at the testing and evaluation of reflectance and BDF models through comparisons with actual measurements. Obviously, these models can be verified by comparing their readings with actual measurements performed on real materials. However, in order to obtain the readings from the computer models in the first place, one must perform a computer simulation of the inputs and outputs of the model, *i.e.*, considering light incident from a given direction and at a given wavelength, one must measure the spectral and spatial distributions of that light after being processed by the model. These measurements are performed using a virtual device, or a computer simulation of a real measurement device, whose formulation should reproduce actual measurement conditions as faithfully as possible to minimize the introduction of bias in the comparisons.

It may be argued that wildly different computer models can provide the same reflectance for a given illuminating, or incidence, geometry. However, for practical purposes the evaluation of a computer model will take into account how close, quantitatively and qualitatively, the overall

curves provided by this model are from the actual curves for different measurement instances. For example, suppose that the spectral curves provided by a reflectance model A have an average discrepancy of 5% with respect to the actual curves, and the curves provided by a model B have an average discrepancy of 30%. Which one should be incorporated into a rendering framework?

The second application corresponds to data generation from previously validated computer models. This may involve a large number of measurements with respect to different wavelengths and illuminating geometries. Such data can sometimes be found in the literature where actual measurements from real materials are reported. However, more often it is not available, and even when it is available, it is only for a restricted number of measurement configurations. For example, the most comprehensive set of experiments involving leaf optical properties performed to date [101] was limited to a single angle of incidence, 8°.

Virtual measurement devices are usually described in connection with a scattering model when they are discussed in the computer graphics literature. For example, Gondek *et al.* [80] have used a device for spectral and spatial measurements, a virtual goniospectrophotometer, presented as an optics model and a capture dome used in conjunction with a geometric model of surface microstructure. In this chapter the formulation of virtual measurement devices is described independently of the reflectance and scattering models.

3.1   Virtual Spectrophotometry

There are many scattering models in the computer graphics literature classified as reflectance and transmittance models. This classification is in many cases not entirely accurate since they only compute the BRDF and BTDF using reflectance and transmittance values, which correspond to input data, as scaling factors or "weights", for the spatial distribution of the scattered light. For example, the models described in Chapter 6 and Chapter 8 can be used to render a plant leaf under different lighting conditions, provided foliar reflectances and transmittances for different wavelengths and illuminating geometries are available as data for the model.

The data for these models [93], is, in general, not available. This

highlights two important issues related to biologically and physically-based rendering. First, it shows the need for developing models to compute reflectances and transmittances, specially for organic materials. Second, it shows the need for developing accurate and efficient measurement procedures, as pointed out during the *Workshop on Metrology and Modeling of Color and Appearance*[1].

3.1.1 Characteristics of Actual Spectrophotometers

A spectrophotometer is defined to be any instrument for measuring the spectral distribution of reflected and transmitted radiant power, and spectrophotometry is defined as the quantitative measurement of reflection and transmission properties as a function of wavelength [59]. Spectrophotometers can also be used to determine the absorption characteristics of an object as a function of wavelength. For applications involving organic materials (*e.g.*, precision farming and plant physiology studies), however, the measurement of absorption profiles is often performed directly with fiber optics microprobes [108].

Actual reflectance measurements are usually performed under illuminating and viewing conditions recommended by CIE[2]: $45°/0°$, $0°/45°$, *diff*$/0°$ and $0°/$*diff* (Figure 3.1), where *diff* stands for diffuse. The first three conditions give reflectance (radiance) factor readings, and the last one gives reflectance readings. We note, however, that the numerical values of reflectance and reflectance factor are identical under the conditions of hemispherical collection.

Integrating spheres are used to provide readings where either the illuminant or viewing specification is "total" or "diffuse only". A gloss trap may be incorporated in the design of the integrating sphere to reduce the influence of the specular component of specimens with mixed reflection behavior. According to CIE, in the $45°/0°$ and $0°/$*diff* conditions, specimens with such behavior should not be measured with strictly normal illumination in order to reduce the possibility of introducing systematic errors, which may be caused by interreflections between the specimen and the emitter device. CIE recommends, however, that the angle between the direction of viewing and the normal to the specimen should not exceed $10°$, and the angle between the axis and any ray of an illuminating beam

---

[1]http://slp.nist.gov/appearance/workshop.html
[2]Commission Internationale de L'Eclairage.

should not exceed 5° [110].
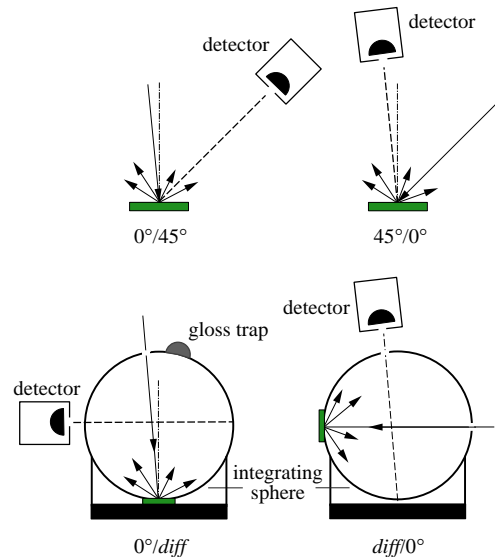
Figure 3.1: Typical illuminating and viewing measurement conditions recommended by CIE for the colorimetric specification of opaque specimens.

The transmittance of translucent specimens depends greatly on the way they are illuminated and mounted in the instrument. Generally transmittance measurements are carried out with the sphere-type spectrophotometers. For plant specimens the transmittance is usually measured by placing the specimen at the port of entrance of the instrument [108] (Figure 3.2). There are a number of detailed issues specific to performing spectral measurements for translucent materials which are beyond the scope of this book. For a comprehensive discussion of these issues the interested reader is referred to the report by Aydinli and Kaase [8].

The 0°/45° (45°/0°) type spectrophotometers have been manufactured with specimen areas up to approximately $50mm$ in diameter, and a typical sphere-type spectrophotometers exposes a smaller flat area of specimen, roughly $25mm$ in diameter for measurement [102]. An integrating sphere may be of any diameter provided that the total area of the ports does not exceed 10% of the internal reflecting sphere area [110].

Although there is no material with properties of a perfect reflecting
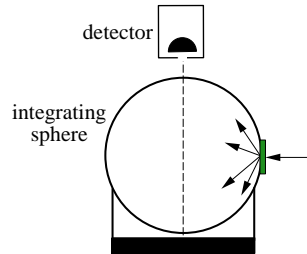
Figure 3.2: Typical measurement of directional-hemispherical transmittance.

diffuser, it is possible to calibrate suitable "working standards", such as magnesium oxide (MgO) powder or barium sulfate ($BaSO_4$) powder, which are often used to cover the integrating sphere wall. For absolute measurements, the sphere wall is the standard, and the integrating sphere theory [76] compensates for the absolute reflectance of the sphere wall by mathematically treating the wall reflectance as unity, since the spectral reflectance of such working standards varies somewhat with the wavelength (around 0.970 to 0.985 in the visible region of the light spectrum [110]). Hence, the hemispherical measurements made with such integrating spheres correspond to absolute values of reflectance (or transmittance), which are subject to small errors associated with factors such as aperture losses, small values of non-uniformity of sphere wall reflectance and stray reflectance from sample mounts [212]. A typical spectrophotometric record of reflectance measurements is illustrated in Figure 3.3.

The precision of a spectrophotometer is estimated by the ability of the instrument to replicate a measurement for a given specimen under same spectral and geometrical conditions [110]. The best-designed, best-constructed, and best-calibrated spectrophotometers still yield results from the same specimen that differ from one measurement to the next. According to MacAdam [135], the differences among readings should be quite small and randomly different. These differences, or uncertainties, are net results of combinations of many small fluctuations due to mutually unrelated variations of different components of the instrument, different factors in the environment and how the specimen is handled. In theory, a spectrophotometer is considered to be of high precision if the spectral measurements have an uncertainty, υ, of approximately ± 0.001 [110, 135]. This means that at one time the device may read, for instance, a
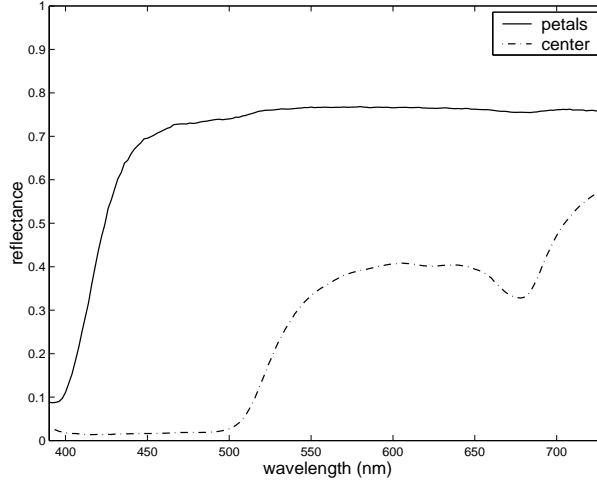
Figure 3.3: Reflectance spectra for a daisy flower (*Bellis perennis*) formed by a yellow center and white petals [203].

reflectance value equal to 0.375, but at other times it may read values as low as 0.374 or as high as 0.376. In practice, however, spectrophotometers usually have an absolute precision between 0.993 and 0.995, *i.e.*, an uncertainty between ±0.007 and ±0.005 measurement units [212]. The accuracy of a spectrophotometer is measured by the ability of the device to provide, for a given illuminating and viewing geometries, the true spectral reflectance and transmittances of a given specimen, apart from random uncertainties occurring in repeated measurements [110].

3.1.2 General Formulation of Virtual Spectrophotometers

Emitters and specimens used in actual measurements usually have circular areas [52, 76, 101, 212], which can be represented by disks with radii r_1 and r_2 separated by a distance D (Figure 3.4). A spectrophotometer with integrating sphere is simulated by sending (or shooting) sample rays from the emitter towards the specimen. These rays arrive at the specimen through a solid angle, $\vec{\omega}_i$, in the direction of incidence ψ_i, which is given by a pair of spherical coordinates (ϕ_i, θ_i) (Figure 3.4). We denote the total number of sample rays used in a virtual spectrophotometric measurement by N.

Consider N rays shot towards the specimen for a given wavelength λ.
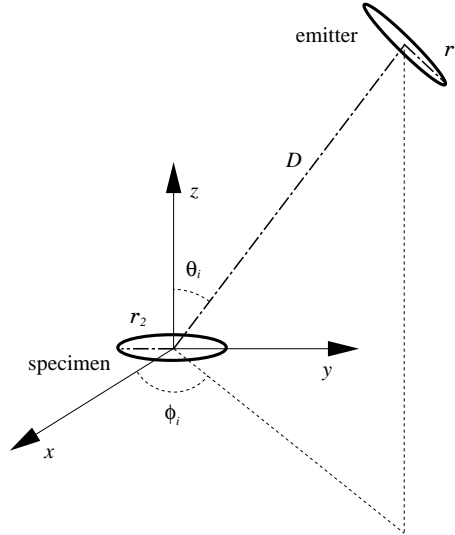
Figure 3.4: Sketch of a virtual spectrophotometer.

One can assume that each ray carries the same amount of radiant power, Φ_{ray}. If the total radiant power to be shot is Φ_i, then the radiant power carried by each ray is given by [172]:

$$\Phi_{ray}(\lambda) = \frac{\Phi_i(\lambda)}{N} \tag{3.1}$$

Recall that reflectance describes the ratio of reflected power to incident radiant power, and transmittance describes the ratio of transmitted radiant power to incident power [151]. Considering this ratio, if n_r rays are reflected towards the upper hemisphere Ω_r, the reflectance of the specimen with respect to a given wavelength λ of the incident light will be given by:

$$\rho(\lambda, \vec{\omega_i}, \Omega_r) = \frac{n_r}{N} \tag{3.2}$$

Therefore, since one can simply count the number of rays reflected to the upper hemisphere to determine a specimen's reflectance, a virtual spectrophotometer does not need to use an integrating sphere to collect the reflected rays. The specimen's transmittance is calculated in a similar manner, *i.e.*, by counting the number of rays transmitted to the lower hemisphere.

Model dependent issues, such as the use of weights associated with rays, will not be dealt with in this chapter. In the same way that an

actual spectrophotometer is completely independent of how the specimen interacts with light, a virtual spectrophotometer shall also be independent of the reflectance model being tested. Moreover, these weights are usually based on reflectances and transmittance values. As mentioned before, if we knew these values *a priori* there would be no need to carry out spectrophotometric measurements.

For applications involving data generation from a previously validated model, the sample rays are collimated since we are basically measuring directional-hemispherical reflectance [151]. In this case, the sample rays have the same origin and hit the specimen at the same point. For applications involving comparisons with actual measurements, as mentioned earlier, the actual measurement conditions must be reproduced as faithfully as possible. In these situations we are measuring conical-hemispherical reflectance [151], which requires the generation of sample rays distributed angularly according to the geometrical arrangement of the surfaces used to represent the emitter and the specimen. As mentioned by Crowther [52], the incident radiation from an emitter shows no preference for one angular region over the other. So, in order to simulate these measurement conditions, the origins and targets of the rays are random points (or sample points) chosen on the disks used to represent the emitter and the specimen respectively.

There are many sampling strategies that can be used to select the sample points on the disks [172, 176]. In this book we do not intend to determine the most accurate or the most efficient one. The merits and drawbacks of different sampling strategies have been adequately covered elsewhere [75, 176, 175, 178].

For the sake of completeness, we outline two strategies that can be used in these applications. One of them is based on standard random sampling [172]. It consists of generating sample points inside a square with sides $2r$ and throwing away points lying outside a disk of radius r inscribed in the square [52]. The sample points in the square are generated using uniformly distributed random numbers ξ_1 and ξ_2 on the interval $[0, 1]$ and the following transformation:

$$(x, y) = r(2\xi_1 - 1, 2\xi_2 - 1) \tag{3.3}$$

where the pair (x, y) corresponds to the coordinates of a sample point.

Another strategy that can be used in virtual measurements is based on the classical Monte Carlo stratified sampling or jittered sampling [172].

It uses a warping transformation to guarantee that the sample points are reasonably equidistributed on a disk, and enables the computation of the pair (x, y) through the following warping function:

$$(x, y) = (2\pi\xi_1, r\sqrt{\xi_2}) \tag{3.4}$$

After generating the x and y coordinates of a sample point, for example using either approach mentioned above, the z coordinate is added. For a sample point on the specimen, z is equal to zero, and, for a sample point on the emitter, z will correspond to the distance D between the disks (Figure 3.4), which is given by the radius of the integrating sphere of a real spectrophotometer. Finally, to obtain the origin of a sample ray, the corresponding sample point (x, y, z) on the emitter shall be rotated according to a specified incidence geometry given by ϕ_i and θ_i (Figure 3.4).

3.1.3 Practical Issues

The main question to be addressed when performing a virtual spectrophotometric measurement is how many rays should be cast by the emitter element, that is, how large should N be. Using a sufficiently large number of sample rays, one will have a high probability to obtain estimates within the region of asymptotic convergence of the expected value of reflectance, or transmittance, being measured according to the Bernoulli theorem [192, 37, 36].

However, as shown by numerical experiments presented by Baranoski *et al.* [15], the processing time grows linearly with respect to the total number of sample rays N since the cost of the algorithm is constant per ray. In order to minimize these computational costs Baranoski *et al.* proposed a bound on the number of sample rays derived from the *exponential* Chebyshev inequality [180]. This bound is given by:

$$N = \left\lceil \frac{\ln(\frac{2}{\delta})}{2\upsilon^2} \right\rceil \tag{3.5}$$

where δ corresponds to the confidence on the estimation, and υ represents the uncertainty of the real spectrophotometer whose readings one intends to compare the virtual measurements with. For example, considering a confidence of 0.01 (humans do not perceive variations of light smaller than 1% [152]), and an uncertainty of 0.005, $10^{5.02}$ rays are required to obtain

reflectance and transmittance readings within the region of asymptotically convergence.

3.2 Virtual Goniophotometry

Virtual goniophotometric measurements allow the determination of the scattering profile of specimens. These measurements can also be used to verify the physical characteristics of the computer model used to simulate such scattering profile. Among these characteristics we can list reciprocity, energy conservation and anisotropy.

3.2.1 Characteristics of Actual Goniophotometers

A goniophotometer is defined as an instrument that measures flux (power) as a function of angles of illumination and observation [59]. This instrument is important in remote sensing research, illumination research and other scientific areas where the flux distribution is important. The measurements made by a goniophotometer can be performed in different ways, and, as a result, there are many possible configurations for these devices. Computer graphics researchers have proposed extensions for industry made goniophotometers [62] as well as designs based on the use of digital cameras [114, 205]. A review of these devices is beyond the scope of this book. A reader interested in a detailed description of goniophotometers used in computer graphics is referred to more comprehensive works in this area [62, 139].

Two photographs of a goniophotometer are shown in Figure 3.5 where it depicts the usage of the instrument by Combes *et al.* [47] to compute BDFs of plant specimens. The light flux incident on the specimen comes from an emitter and is captured by a detector (photometer) after being reflected or transmitted by the specimen. For BRDF measurements the detector(s) are placed in hemisphere above the specimen (Figure 3.5 left) and for BTDF measurements the detector(s) are placed in hemisphere below the specimen (Figure 3.5 right).

In order to obtain a complete goniophotometric record for a simple specimen it would be necessary to perform a formidable number of measurements as mentioned by Judd and Wyszecki [110]. Both the emitter and the photometer would have to be moved independently of one another to every position on the hemisphere. In order to illustrate this aspect Judd
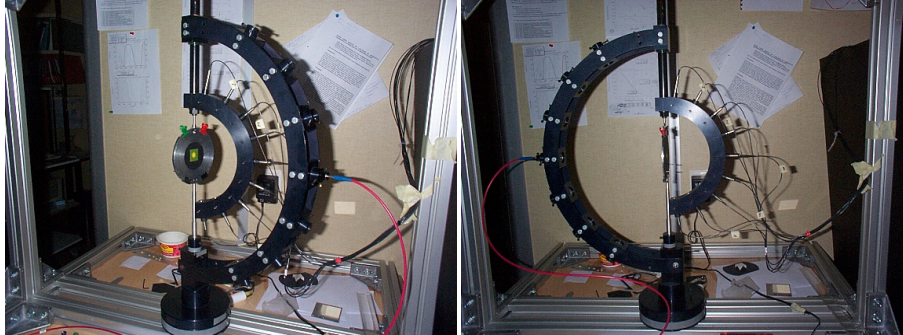
Figure 3.5: Photographs of a goniophotometer showing different set-ups for BRDF (left) and BTDF (right) measurements. (Courtesy of Stephane Jacquemoud.)

and Wyszecki perform the following calculation. Suppose that one works with a fairly large solid angle of approximately 0.005 steradian for each aperture. To cover the entire hemisphere (2π steradian) as closely as possible with such an aperture without overlapping, we must use about 1000 different positions. With both the source and the photometer moved in each of the 1000 positions one ends up making 1 million measurements!

A typical three dimensional representation of a goniophotometric record of BRDF measurements is shown in Figure 3.6. For many specimens the most informative goniophotometric data are taken in the plane containing the direction of the incident light and the normal of the specimen. Many actual goniophotometers are abridged to this extent. The emitter movement is from $\theta_i = 0°$ to $\theta_i = 90°$ and the photometer movement ranges from $\theta_r = 90°$ to $\theta_r = -90°$. Assuming the same aperture sizes as before, this abridged goniophotometric record would contain $18 \times 36 = 640$ data points. Like the accuracy of spectrophotometers (Section 3.1.1), the accuracy of a goniophotometer is also estimated by the ability of the instrument to replicate a measurement for a given specimen under same spectral and geometrical conditions [110]. According to data provided in the measurement literature [62], the uncertainty of actual goniophotometers is usually around 0.5% or higher.

3.2.2 General Formulation of Virtual Goniophotometers

In order to simulate radiance measurements performed by placing a photometer at different viewing positions, one can use radiance detectors,
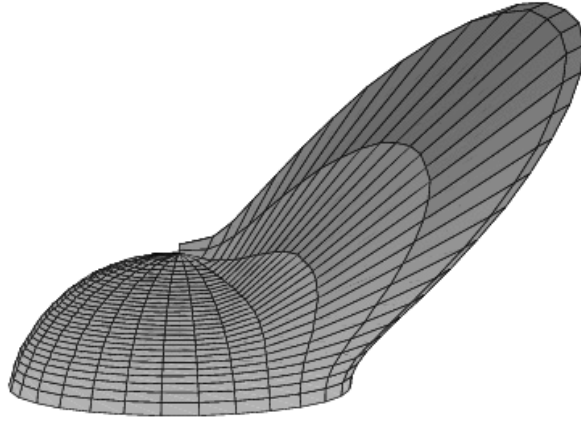
Figure 3.6: Three dimensional representation of the BRDF of a glossy specimen, *i.e.*, a material with mixed reflection behavior.

which are represented by the patches of a collector sphere placed around a specimen. Figure 3.5 presents a sketch showing the principal components of a virtual goniophotometer and their geometrical arrangement. The light flux incident on the specimen comes from the emitter through patch I, and the light flux is collected by the photometer covering patch V. Both of the illuminating and viewing directions can be varied independently within the hemisphere above the specimen. The position of emitter and patch I is given by the azimuth angle ϕ_i and the polar angle θ_i. The positions of the photometer and patch V are given by the azimuth angle ϕ_r and the polar angle θ_r.

Using this arrangement, the BRDF for a direction associated with a given radiance detector placed in the upper hemisphere can be determined in terms of radiant power. More specifically, it is given by the ratio between the radiant power reaching the detector, Φ_r, after interacting with the specimen, and the incident radiant power, Φ_i [81].

The corresponding expression used to compute the BRDF for light incident at wavelength λ, considering the solid angle in the direction of incidence, $\vec{\omega_i}$, and the solid angle in the direction associated with the radiance detector, $\vec{\omega_r}$, is given by:

$$f_r(\lambda, \vec{\omega_i}, \vec{\omega_r}) = \frac{\Phi_r(\lambda)}{\Phi_i(\lambda) \, \vec{\omega_r}^p} \tag{3.6}$$
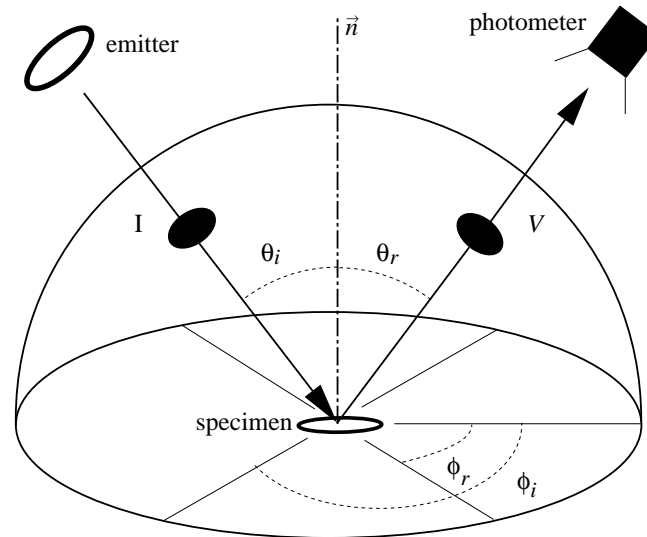
Figure 3.7: Sketch of a virtual goniophotometer.

where:

$\vec{\omega_r}^p$ =   projected solid angle with respect to the direction associated with the radiance detector.

In turn, the projected solid angle $\vec{\omega_r}^p$ is given by:

$$\vec{\omega_r}^p = \frac{A_r \cos \theta_r}{D_r^2} \tag{3.7}$$

where:

A_r	=	area of the radiance detector,
D_r	=	distance from the specimen to the radiance detector,
θ_r	=	angle between the direction associated with the
		radiance detector and the specimen's normal.

Recall that the radiant power reaching the radiance detector can be written as:

$$\Phi_r(\lambda) = n_d \Phi_{ray}(\lambda) \tag{3.8}$$

where:

n_d	=	number of rays hitting a radiance detector.

Thus, replacing Equation 3.1 and Equation 3.8 in Equation 3.6, the expression to compute the BRDF reduces to:

$$f_r(\lambda, \vec{\omega_i}, \vec{\omega_r}) = \frac{n_d}{N \, \vec{\omega_r}^p} \tag{3.9}$$

Similarly, the BTDF is calculated considering radiance detectors placed in the lower hemisphere.

The origins of the rays are random points uniformly chosen from a disk used to represent the surface of the emitter. The coordinates of the points are given by pairs (x, y), which are computed using the warping function given by Equation 3.4. The targets of the rays may also be random points uniformly chosen from a disk used to represent the specimen. Alternatively, we can use a pair of triangles used to represent it. In this case, to choose a random point q on a triangle defined by the vertices q_0, q_1 and q_2 we can use the following expression:

$$q = q_0 + x'(q_1 - q_0) + y'(q_2 - q_0) \tag{3.10}$$

where x' and y' are obtained using another warping function suggested by Shirley [172]:

$$(x', y') = (1 - \sqrt{1 - \xi_3}, (1 - x')\xi_4) \tag{3.11}$$

where:

ξ_3 and ξ_4 = uniformly distributed random numbers $\in [0, 1]$.

3.2.3 Practical Issues

Krishnaswamy *et al.* [120] examined the implementation of virtual goniophotometric devices focusing on the subdivision of the collector sphere and on the ray density required to obtain asymptotically convergent BRDF and BTDF estimates. Their experiments indicated that the use of a subdivision technique based on equal project solid angles may provide a more uniform convergence for the estimates, and an upper bound for the number of rays can also be derived from the exponential Chebyshev inequality. This bound is given by:

$$N = m \left\lceil \frac{\ln(\frac{2}{\delta})}{2v^2} \right\rceil \tag{3.12}$$

where m gives the number of patches on the collector hemisphere, δ corresponds to the confidence on the estimation, and v represents the uncertainty of the real goniophotometer whose measurements one intends to compare the virtual measurements with. For example, considering a confidence of 0.01, an uncertainty of 0.005 and $m = 900$ patches, at most 10^8 rays would be required to obtain asymptotically convergent BRDF and BTDF estimates.